Vol. 43, No. 1 (2021) 66-82, DOI: 10.24874/ti.973.09.20.01

Tribology in Industry

www.tribology.rs

RESEARCH

Tribo-Modeling of Drilling Processes

G.S. Panagopoulos[a], P.G. Nikolakopoulos[a,*]

[a] *Machine Design Laboratory, Department of Mechanical and Aeronautical Engineering, University of Patras, Rio Patras, Patras 26500, Greece.*

Keywords:

Drilling
FEM
Coating
Wear
H-13
WC
Adhesion
Temperature

* Corresponding author:

Pantelis G. Nikolakopoulos
E-mail: pnikolakop@upatras.gr

Received: 29 September 2020
Revised: 24 October 2020
Accepted: 18 January 2021

A B S T R A C T

The purpose of this paper was to investigate the wear rate and the temperature distribution of a single-layer TiN coated drill in H13 steel alloy workpiece, with the use of a numerical procedure and through relevant experiments. Simulation models were developed, and an experiment was conducted to evaluate the wear rate, as well as the wear mechanisms and the temperatures appeared during the process of drilling. The finite element method was used to simulate the drilling process. The Usui wear model was used for the drill's wear rate estimation. Temperature measurements were carried out with a thermal imaging camera, and SEM microscopy was also used to characterize the coating's wear. The maximum wear rate of the drill either of flat or for angled simulation setups is near $0.005\,\mathrm{mm/sec}$. *This value is obtained for maximum tool temperature, which in both cases is close to* $140^{\circ}\mathrm{C}$, *however with different distribution within time. The comparative analysis of the simulation models and the experiment show that adhesion is the dominant wear mechanism and the values of the temperature are in good agreement (*$5^{\circ}\mathrm{C}$ *difference) between the model and the measurements, even after the process temperature measurement. Because of the good chip evacuation and chip length the coated drills are suitable for drilling tough materials.*

1. INTRODUCTION

In the turn of the twentieth century, High Speed Steel (HSS) was introduced as cutting steel, which promoted drill performance, and along the twist geometry it became widely used in the need of drilling holes. Its significance has long been recognized due to the need for a large number of holes to be drilled on engineering components and the large amount of costs involved in the process. For instance, building an Airbus A350 aircraft can require up to 55.000 holes. According to Tönshoff *et al.* [1], drilling comprises approximately 30% of all metal cutting operations and along with processes like reaming or tapping it is often the operation that determines the shortest cycle time in production lines, and it is in the first place regarding the number of working steps. Even a slight increase in the general level of the drill's performance could be very profitable for individual firms or industries as a whole either on an economical or practical level. Also, drilling is carried out as one of the last steps in manufacturing and it is

therefore essential to ensure that the process is performed with reliability, as it is often the case that the part has undergone extensive machining already. Thus, poor drill performance can result in production waste which can be very costly for industries.

Furthermore, there are some inherent weaknesses in the conventional twist drill design which lead to poor cutting action, large cutting forces, low production rate, possible drill breakages inside the workpiece and rapid tool wear. Tool wear is strongly correlated with tool life, as well as the surface roughness and geometric tolerances of the final product. These aspects are evident in the machining of difficult-to-cut materials such as nickel or titanium alloys as reported by Ezugwu and Lai [2]. Materials of these types are frequently used in applications that require high fatigue strength and good corrosion resistance, however those same characteristics become a problem during machining operations. It is worth mentioning the example of drilling process on the nickel-based superalloy inconel 718. This particular material is a high temperature precipitate-hardening alloy. Due to its excellent mechanical properties in a wide range of temperatures (-250 to 700 °C), it is usually applied in very demanding working environments, such as nuclear energy or petroleum industries. During the operation of drilling this superalloy, the tool temperature rises easily and proportionally to the cutting conditions, and micro welding in the tool tip takes place because of the high forces and the excessive friction as mentioned by Chen *et al.* [3]. This can lead to discrepancies in the geometry of the part, as the tool tip has changed in size. Furthermore, the material's properties result in a difficulty breaking the generated chip during process.

The existing modifications to the twist drill design, albeit successful in reducing the thrust forces, show limitations in reducing the drilling torque and power required. The twist drill geometry has been subject to numerous investigations which are intended to improve its general function, has been analyzed widely and has been described in many international standards. In the late 1970s, thin layers of hard and wear resistant coatings, such as black oxide, titanium nitride (TiN) or Zirconium nitride were used on cutting tools to increase their durability and tool life while reducing the tool-workpiece and tool-chip friction forces. These types of coatings have been proved to be some of the most important innovations, not only in twist drills, but broadly in cutting tools technology. Later on, there is a brief reference about coatings.

There have been many articles and academic research papers published regarding machining. Most of them deal with the problems of wear and friction generated during the first, as well as the optimization of specific processes and geometry of tools.

Jafarian *et al*. in [4] investigated the surface quality and geometrical characteristics in the drilling of H-13 steel. They conducted experiments and developed an optimization algorithm in order to choose the optimum cutting conditions in the process of drilling. They concluded that high depth of cut, feed rate and tool diameter improve the surface quality and circularity of the produced holes.

Similar geometry characteristics were also studied in [5] by Ganesh *et al.* In their study, a coated carbide twist drill with 12 mm diameter was implemented for drilling H-13 steel. In this case, the researchers conducted experiments and utilized the Taguchi method and analysis of variance to find the dominant parameter affecting the surface roughness of the produced holes. Apart from that, optimization of the cutting conditions as a mean of improving the power utilization and tool life was also achieved via their study.

The relationship of cutting forces and hole quality was examined by Tekaüt *et al.* in [6]. In this study, the authors conducted experiments in a vertical machining center with coated and uncoated carbide drills in order to check the hole quality with regard to the generated cutting forces. It was found that lower cutting forces were developed in the case where coated drills were used. In addition, the coated drills resulted in better geometry, surface roughness and chip evacuation during process.

The same authors in [7] examined the relationship between the cutting conditions and the temperatures generated on coated and uncoated carbide tools during drilling of H-13 steel. They concluded that higher feed rates and cutting speeds led to a decrease in temperatures. Also, higher temperatures were observed on coated drills due to lower heat conduction.

In [8], Brandao *et al.* conducted drilling experiments on H-13 steel with the use of carbide drills, in order to record and evaluate the drilling temperature under different tribological conditions, namely dry, flooded and minimum quantity of lubrication (MQL). They concluded that the temperature decrease was proportional to the amount of lubricant applied, and MQL temperatures were significantly lower compared to those of dry cutting.

The same author in [9] evaluated the hole quality during high speed drilling of hardened H-13. They used new and worn out TiAlN drills with different cooling methods and different cutting speed. They concluded that dry drilling gives the worst results. In addition, higher speeds are no beneficial for diameter and circularity errors, and show no important difference in surface roughness or cylindricity. Cylindricity is affected mainly by cooling and lubrication, despite the drill's wear. Thus, high cutting speed with use of cooling and lubrication produces the best hole quality.

Lauro *et al.* in [10] examined the heat flow during drilling of H-13 steel of 52 HRC, with different types of cooling and lubrication, and with use of TiAlN coated drills. Also, they developed finite element models (FEM) to define the heat flow and the coefficient of convection for their systems. They found that the simulation models yielded results close to the experimental, and also that (MQL) cooling is more effective than that of the flooded system.

Coldwell *et al.* [11], studied rapid machining techniques on hardened H-13 moulds and dyes. They extended their research on the drilling capabilities on H-13. They found that carbide tooling can produce up to 210 holes of 16 mm depth with $Vc = 30\,\mathrm{m/min}$ and $f_{rev} = 0.1\,\mathrm{mm/rev}$.

Tekaüt *et al.* in [12] evaluated different cutting parameters in drilling of H-13 steel in soft and annealed condition with the use of coated and uncoated carbide twist drills. They concluded that an increase in cutting speed leads to high stresses and higher wear values for the uncoated drills, especially on drills' center, because of their difficulty to evacuate the produced chips. In contrast, elevated speeds did not affect the coated tools in the same way due to the coating material, and the fact that chips were disposed faster and easier via the tools' flutes.

Wu and Han experimentally evaluated the temperatures during dry drilling [13]. They developed simulation models in several software modules and they concluded that the simulation results yield errors of less than 15% in comparison to the experimental ones.

Bono and Ni in [14] analyzed the temperature profile along the edges of a twist drill. They developed simulation models in which the heat flux is determined from analytical equations. The simulation results showed that higher temperatures occur on the chisel edge of the tools, which are attested with experiments.

In the above studies, the main wear mechanism discussed was adhesion. Also, what is more interesting is the fact that despite changes in the cutting lips' geometry of the drill, flank faces tend to be prone to wear, determining the drills' lifespan. In addition, flaking is very typical in most of the drills' periphery due to the 'aggressive' rake angle they are grinded with.

Apart from the studies showed above that concern drilling in difficult to cut materials either experimentally or via simulation and experiments, there have also been publications aiming at the carbide wear in machining. Epigrammatically, it is worth mentioning the papers published by Lorentzon and Järvstråt regarding the modeling of tool wear in cemented carbide when machining inconel 718 the year 2008 [15].

In these studies, the main target was to develop an FE model that will be able to predict carbide tool wear when machining nickel-based alloys. To perform this, many parameters were investigated such as heat generation, while a large number of mathematical models were used. They concluded that the Coulomb friction model they used along with the Usui's wear equation that is presented later in this study, show good agreement with experiments.

In the present work, the wear mechanisms which are implemented during the process of tough metals' drilling, such as H13 steel, with the use of a coated WC twist drill are examined and discussed. Additionally, the temperatures

generated during friction coupled forces model on both the workpiece and the tool have been taken into account and examined. From the literature, it was evident that finite element modeling regarding H-13 drilling is limited. The main contribution of this work is the finite element modeling of the tungsten carbide (WC) drill that penetrates in H-13 work piece, in combination with experimental temperature measurements and SEM microscopy in order to see the physics and the wear mechanisms behind the drill processes. The friction couple model is developed with use of DEFORM-3D software. The Coulomb friction model and the Usui wear models are used in order to estimate the drill's tribological behavior. The results acquired confirmed that the experimentally obtained data are in agreement with the predictions from the simulation models.

2. GEOMETRICAL AND THEORITICAL CONSIDERATIONS.

The nomenclature of a common twist drill and its main features is the following: Axis, Body, Shank, Drill diameter, Drill margins, Web, Chisel edge/ Chisel edge angle, Flutes/ Flute length, Land, Helix angle, Drill points, Lip relief angle, Flank faces, and the Rake angle. These features are illustrated in Fig. 1.

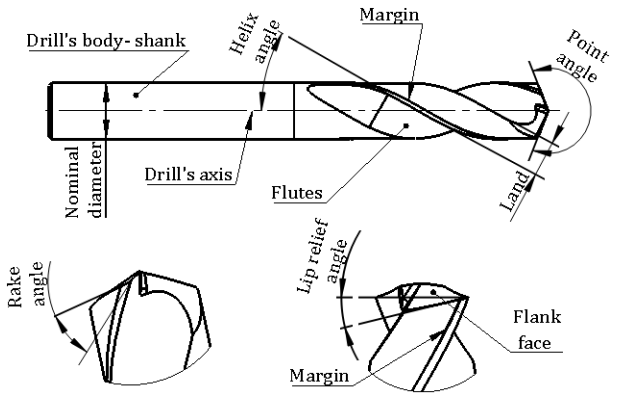

Fig. 1. Geometric features of a split point twist drill [16].

As a result, the most prominent drill point features in order to describe its geometry are the nominal diameter D, the point angle which is usually symbolized as $2p$, the chisel edge angle ψ, the web thickness $2W$ (or web thickness ratio $2W/D$), the helix angle δ_0 and the lip clearance (relief) angle α_0.

In the current study, a commercial high-performance split point twist drill is used. The cutting edges of the drill are illustrated in Fig. **2**. With a split-point drill bit, chisel edge length is reduced significantly and as a result, the required thrust force for the drill to enter the material is also reduced. The web of the drill has a small radius and is suitable for high strength steels. A lack of symmetry in the cutting edges of a split point drill yields unbalanced forces during drilling, higher wear rates and oval bore.

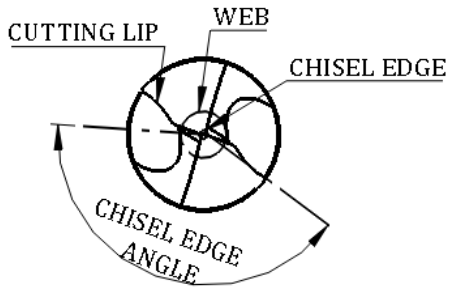

Fig. 2. Split point drill tip.

Also, the tool is made out of solid tungsten carbide, with 10% cobalt and TiN coating. Generally, this type of coating yields good wear resistance [17], with low friction coefficients which results in very good surface finish, low power consumption, high hardness and adhesion on the substrate of the tools. In addition, it can be used in elevated temperatures with good corrosion resistance.

Furthermore, the mechanical properties of TiN coating are a function of its microstructure. Microscopically, TiN coating is composed of columnar grains with size between 1-3mm. Another aspect of the TiN structure is the stoichiometry on which the deposition process plays a major role. The coating colour depends on the atomic ratio of Ti, but what is more important is that the mechanical properties such as microhardness and adhesion are a derivative of this. The coatings' hardness is measured with the use of the respective laboratory apparatus and can be calculated experimentally with the following equation:

$$H_c = \frac{V_f}{V_t} H_f + \frac{V_s}{V_t} c^3 H_s \qquad (1)$$

where H_f is the hardness of the film of the tester, V_f is the film volume and V_s the substrate volume with respect to the total volume V_t, H_s is the

hardness of the substrate, and c an interface parameter. Accordingly, adhesion is measured with similar equipment, which in this case is a scratch tester.

The performance of a twist drill can be determined from a variety of variables such as thrust force or torque needed, good hole tolerances and surface finish, and drill life. In order to evaluate a drill's performance, these variables need to be studied and taken into account. This, along with the fact that many different materials require to be tested, makes the evaluation relatively laborious. Numerous researchers, such as E. Armarego in [18] or Endres W J *et al.* in [19] have applied the mechanics of cutting approach in order to predict the force and torque required during the drilling processes. The mechanics of cutting approach is based on the classic orthogonal and oblique cutting models. Many researchers used these two models in different ways, and they created equations with different parameters. However, none of these were exact and reliable as to their use, because there are many variables that should be considered during the drilling processes.

After many modelling approaches, E.J.A. Armarego [18] formed the "Unified-generalized mechanics of cutting approach". This model of cutting approach has been proven to be accurate for a wide range of machining fields such as milling, turning or drilling, where in each case different parameters are implemented.

It is known that the traditional chip formation process consists of a shearing process in localized thin shear zone along with the friction process taking place in the tool-chip interface. However, extensive experimental research on both classic orthogonal and oblique cutting proved that a third parameter should be also taken into account. This is called 'edge' force components and is caused due to rubbing and ploughing during machining. More specifically, for the oblique cutting operation, the total force components F_p, F_q, F_r according to [18] are:

$$F_p, F_q, F_r = functions(b, t, \lambda_s, \gamma_n, \beta, \tau, C_{ep}, C_{eq}) \quad (2)$$

$$\eta_c = function(\gamma_n, \lambda_s, r_i, \beta) \quad (3)$$

In this functional relationship the parameters included are the following: b is the width of cut, t is the cut thickness, γ_n is the normal rake angle, λ_s is the inclination angle, r_i is the chip length ratio as mentioned earlier, β is the friction angle at the tool-chip interface, τ is the shear stress in the shear zone and finally C_{ep}, C_{eq} are the edge force coefficients. The most significant variables presented above are illustrated in the figure that follows (Fig. 3).

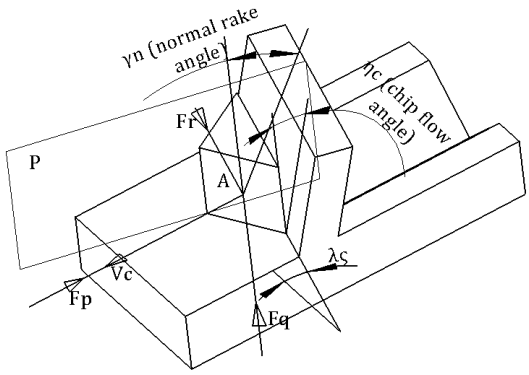

Fig. 3. Generalized oblique cutting process [18].

Concerning friction, the mathematical definition of Coulomb's statement is related to Amontons' equation, and it is:

$$\mu = \frac{F_a}{F_N} = \frac{\tau_i}{\sigma_N} \quad (4)$$

Here, F_N is the normal force at the contact surface, F_a the frictional force due to application of the normal force, τ_i the shear stress on the contact surface and finally σ_N is the normal contact pressure.

The Coulomb model is broadly applied in metal cutting processes. In this work, the present model is selected because it is a fundamental friction law and also, it is the one that DEFORM-3D software uses for friction calculation.

As it is known, friction leads to different types of wear. Many models have been designed to estimate adhesive wear. In 1953, Holm and Archard presented an equation for the calculation of adhesive wear [20]. According to Archard's law, many general models have been created, which are based on the hardness of the adhered material. The worn volume in its simplest form can be expressed as:

$$V = \frac{1}{3}\frac{W_1 L}{H} \quad (5)$$

where V is the volume that is worn, W is the normal load applied, L is the sliding distance and H is the hardness of the material that is worn. In this equation, the worn volume is increased when normal load and sliding distance are also increased and is inversely proportional to the hardness of the material. Also, the tougher the drill's coating the less wear there will be, as suggested by Kato *et al.* in [21]. Usui *et al.* in [22], driven by the basic Archard's law, developed the following equation:

$$\frac{dW}{dt} = C_1 \sigma_N V_c \exp(-\frac{C_2}{\theta}) \quad (6)$$

This equation in known as Usui's Wear model, where Vc is the cutting speed, θ is the temperature during process and the parameters C_1 and C_2 are calculated experimentally. In this work it is used for the calculation for the drills' wear rate as it is more reliable than Archard's equation due to the fact that it uses more data and coefficients related to the materials involved during cutting. Also, Usui's equation provides accurate wear rate values especially for carbide tool wear.

There is a number of different wear types in machining. The majority of those are easily explained for turning based on their appearance, but can also be applied in drilling, with slight modifications. The most common ones are flank wear (like any cutting tool or insert), flaking, and built up edges (smearing), which are mentioned by Dahlström in [23].

Flank wear is the type of wear that occurs on the flank face of the tool due to shear stress from normal pressure while the tool slides over the machined surface. It firstly develops close to the cutting edge, and then grows away from it evenly distributed on the remaining flank face. It is the most typical type of wear that appears during machining. Variations of this can be found which depend on the material that is processed, cutting data and tool shape. For example, smaller lip relief angle on a drill bit is more prone to flank wear due to the higher contact with the machined surface of the material. Other irregularities can be presented because of chipping of cutting edges or influences from crack formations like comb cracks [22].

The flank wear is usually measured according to ISO 3685 standard, which is also mentioned by Grzesik in his book [24], where a VB value is produced, which is the distance measured from the cutting-edge perpendicular to lowest worn area of the tool. Tool life limits often range around approximately 0.3mm for flank wear, and average value for the VB parameter.

Regarding flaking, there are two main locations where it can take place. The first one is inside the coating itself, where parts of it can detach, or in the case of a multilayered coated tool some layers can detach from one another, and the second is flaking amongst the coating and the substrate. There are many parameters that contribute to this type of wear and adhesion of workpiece material that will eventually lead to flaking. The most important of them are the surface properties of the workpiece, elements that correlate with its roughness and its chemical composition, the cutting data which play a major role and finally thermo-mechanical loads that influence the flaking wear especially on intermittent cutting. What is worth noting here is that flaking does not always happen during machining, and it has been observed that the severity of flaking depends mostly on the coating of the tool.

Finally, as for smearing, the main reasons causing this phenomenon are the cutting data that are used, the tools geometry and the work piece properties as well. A typical example is machining of stainless steel, which is a 'sticky' material and can easily form built up edges (BUE). In this case, when the smeared material is detached from the tool, as mentioned earlier it carries fragments from the tool itself, which can be either its coating or its substrate. On severe cutting conditions, the BUE benefit from the friction generated in the tool work-piece interface, and can sometimes weld on the tool. When this happens, not only the tool is worn out, but also the machining process can produce defective parts. The tool's geometry can be subjected to deformations, and the surface finish and heat flow in the cutting zone can also be altered. The smeared mass operates as thermal insulation for the tool, which means that more heat has to be transferred through chips. In this way, new BUE can appear, which makes machining even more difficult. The most efficient method to control and reduce the BUE formation on difficult-to-cut materials is to control the temperature, meaning sufficient lubrication and optimization of cutting data. This work proposes a model for accurate cutting data.

3. MODELLING PROCEDURE

In order to study the adhesive wear mechanism and wear characteristics during the process of drilling, a friction couple model is determined. This means that a specific type of metal with known geometry and mechanical properties is used as the workpiece material and also a drill with known geometry and material characteristics is used as the tool. The friction couple is designed in a 3D CAD system and it is simulated with use of the DEFORM-3D software. Moreover, in order to validate the data collected after the finite element analysis, experiments are conducted under the same cutting conditions.

Regarding the material that is used as specimen, this is H-13 steel, also known as Orvar [25]. This material is used as a tool in quite demanding applications where high thermal loads are applied such as extrusion, plastic moulds or die castings. Also, the yield strength R_p of Orvar is 880MPa and tensile strength R_m is 550MPa in soft annealed condition. The chemical composition and physical data of Orvar are presented in Table 1. As shown, high concentration of Cr is found, which enhances its mechanical properties.

Table 1. Chemical composition of Orvar (table from [25]).

Typical Analysis	C	Si	Mn	Cr	Mo	V
%	0.39	1.0	0.4	5.2	1.4	0.9

3.1. Tool and modelling

The tool that is used plays a major role on the system that is studied. The drill is made out of tungsten carbide (WC) with a single layer coating. A commercial 2 flute drill meeting the above requirements was found, which was manufactured according to DIN 6539. The geometrical characteristics of the drill are presented in Table 2.

Table 2. Geometry characteristics of the used drill.

Geometry characteristics	Symbol	Values
Diameter (mm)	D	10
Point angle	$2p$	140
Chisel edge angle	ψ	60
Web thickness	$2W$	3.05
Helix angle	δ_0	30
Lip clearance angle	α_0	10

Also, the drill is TiN coated. The coating characteristics provided from the manufacturing company are shown in the table that follows (Table 3).

Table 3. Coating properties of the used drill.

Coating Characteristics	Symbol	Values
Coating process	-	PVD
Thickness of coating (μm)	-	1.5-4
Hardness (Vickers)	H	2400
Friction coefficient	μ	0.5

3.2. Friction couple assembly – Cutting Conditions.

The friction couple generated, which in other terms is the workpiece to be processed and the drill, is presented next in Fig. **4**. The Orvar specimen is fixed in space with the appropriate boundary conditions. The cutting tool is placed perpendicular on top of the part, and its cutting edge touches the surface of the part. The feed of the drill is lengthwise its axis, and the boundary conditions used allow it to rotate around it, and move in the Z direction, as shown. The cutting conditions that are used during the process are chosen according to the manufacturer's recommendations for the specified drill series, and are presented on Table 4. Also, the cutting process is dry, which means that no cutting oil or emulsion is used.

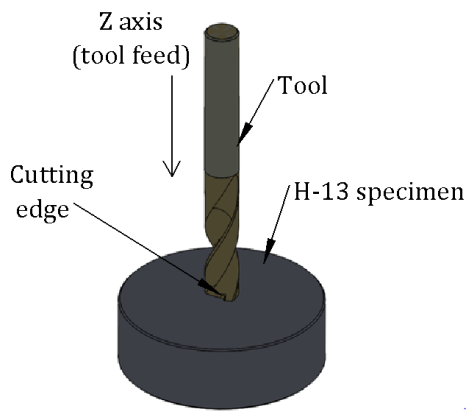

Fig. 4. 3D model of the friction couple that will be studied.

Table 4.Cutting speeds and feeds for the system.

Cutting conditions	Symbol	Values
Cutting speed (m/min)	Vc	40
Spindle speed (rpm)	N	1270
Feed per revolution (mm/rev)	f_{rev}	0.1
Feed per minute (mm/min)	f	127

3.3. Modelling and simulation

In the present study, the FEM software used to model the process of drilling is DEFORM-3D, after an extensive research on different modules of software. The method of solution that DEFORM-3D uses for metal cutting is Lagrangian incremental, and the element types is tetrahedral. In order to acquire the most valid results, a series of analysis was conducted with the same cutting conditions, but different element sizes and number of elements. The final simulation setup is presented in the following charts, i.e. Fig. **5** and Fig. **6**. In addition, in order to get reduced simulation times, the simulations were of two types. In the first setup, only the drill tip dives into the workpiece, while in the second the whole drill geometry is subject to material cutting. The second setup is more preferable in the case of measuring the wear rate in the whole length of the drill's cutting lips. Furthermore, the drill is shortened to 10mm in height, because the rest of the body in the simulation would have no use other than prolonging the analysis time.

Primitively, the type of simulation is chosen, either it is turning, milling, boring, or in this case drilling.

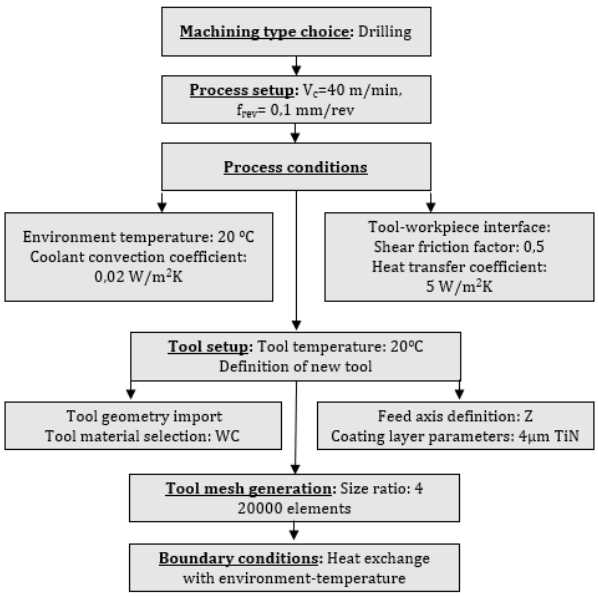

Fig. 5. Flow chart of tool definition and setup in simulation software.

After the simulation type has been selected, the process setup is determined as shown in Fig. **5**. It was earlier proposed that the cutting velocity is $Vc = 40\,\mathrm{m/min}$, and feed rate $f_{rev} = 0.1\,\mathrm{mm/rev}$. Afterwards, the process conditions were entered. In the figure above, it can be seen that the environmental conditions consider that the temperature is $20^{o}\,\mathrm{C}$, which is the approximate temperature in which all machining processes should be conducted in order for the demanded tolerances to be achieved. Also, the convection coefficient of the coolant is $0.02\,\mathrm{N/sec/mm/^{o}C}$. This value is the one that is chosen in the case of dry cutting, and in the present, it is predetermined that wear will be studied in dry cutting conditions, where the only coolant is the still air. The friction factor is $\mu = 0.5$, while the heat transfer coefficient is set to $5\,\mathrm{N/sec/mm/^{o}C}$ for still air.

Subsequently, the tool setup is configured. The drill designed in CAD file is used as tool geometry. In tool setup, the temperature of the tool is set, and finally the position of the geometry is set, with regard to the axis in which the feed will procced for the drill. In the simulation setups for the present study, the Z axis is chosen to be the feed axis. Also, the material the tool is made of is determined, which is WC, and the coating thickness is also set, which is $4\mu\mathrm{m}$ of TiN. Thereinafter, the tool mesh is determined and, in this case, 20000 elements with 4500 nodes are used, in size ratio 4. Size ratio is the edge length of an element in the tip of the tool or workpiece, which is X times smaller than the coarser mesh on the rest of the surface. The minimum element size in the tool's tip is 0.02mm. Finally, for reduced simulation time as said earlier, only the tip of the drill is used as cutting tool in the software, as the rest of the body will not be active.

Next, the boundary conditions for the tool are set, and those regard the heat exchange between the tool and the environment.

Then, the workpiece is defined as it is presented in the flowchart above (Fig. **6**), along with its temperature and its properties. In drilling simulation, the material is considered to be perfectly plastic.

After the workpiece creation, the mesh is done. In this case, a size ratio 10 is used with 71500 elements and 15600 nodes. The software uses size ratio in the workpiece at the position the tool is placed, which is the location where the tool removes material. The default position is the centre of the drill, and the mesh is very fine

in this area in regard to the rest of the workpiece geometry. The minimum element size in the cutting region is 0.03 mm.

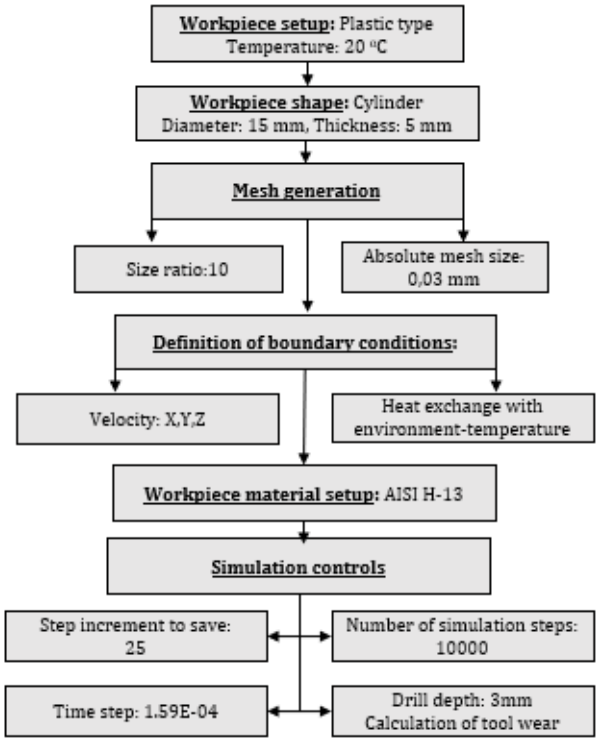

Fig. 6. Flow chart of workpiece definition and simulation setup in the software.

The workpiece mesh is much more complex and problematic than the tools tip, as it deforms during simulation, while the tool is considered as a rigid body [26]. Also, the mesh is automatically regenerated after every time step. The software uses the automatic mesh generation technique (AMG) at every step. After the workpiece mesh has been generated, the boundary conditions of the cylinder are set. In the present simulations the workpiece's velocity is constrained in X, Y and Z axis on the periphery of the cylinder, meaning that it is fixed in space. In addition, the heat exchange with the environment is also set.

In the sequel, the workpiece material is selected. As said earlier, this study examines drilling process on Orvar steel. The flow stress of Orvar tool steel is defined with use of the Johnson and Cook model in the software, which is described from the equation:

$$\sigma = (A + B\varepsilon^n)(1 + C\ln\frac{\dot{\varepsilon}}{\dot{\varepsilon}_0})\left[1 - \left(\frac{T - T_r}{T_m - T_r}\right)^m\right] \qquad (7)$$

where σ is the flow stress, A is the yield stress, B is the strain hardening factor, n is the strain hardening index, C is the strain rate sensitivity parameter, T is the homologous temperature, m is the thermal softening coefficient, T_r is the ambient temperature during simulation, and finally T_m is the melting temperature of the material in process. The flow stress-strain curve for the workpiece material is presented in Fig. **7**.

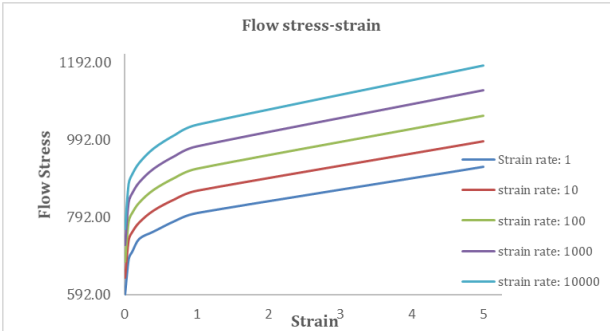

Fig. 7. Flow stress-strain plot for 5 different strain rates.

In the final step, there is the simulation control. Here, the total number of simulation steps is determined to be 10000 steps, with step increment to be saved set to 25, and time step set to 1.59E-04. Also, the desired drill depth that the tool tip should reach is set. This is 3 mm for the tip simulation, and 17 mm for the whole drill geometry. Typically, the simulation steps can be much bigger than the drill depth, as they change according to the mesh size. A finer mesh requires smaller time steps. Also, remeshing criteria can be applied as advanced simulation controls. Generally, the simulation of a drilling problem can take days or even weeks, depending on the computer potential and on the problem setup, as opposed by Berkeley et al. in [26].

Finally, the tool wear calculation is done with use of the Usui model by applying experimental constants according to the material used. There are quite limited resources about these experimental constants, and what is more, only a few types of metals have been examined. As a result, in many cases the default software values are used. In this study the default values for constants C_1 and C_2 will be used, which are $C_1 = 1\text{e-}05$ and $C_2 = 10^3$.

4. RESULTS

4.1 Flat workpiece results

In the first type of setup, where the tip of the drill is entering the workpiece, the temperature is shown in Fig. 8 and Fig. 9.

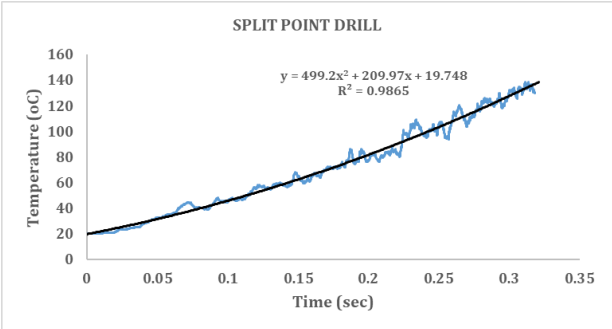

Fig. 8. Temperature during time for the split point tip diving simulation.

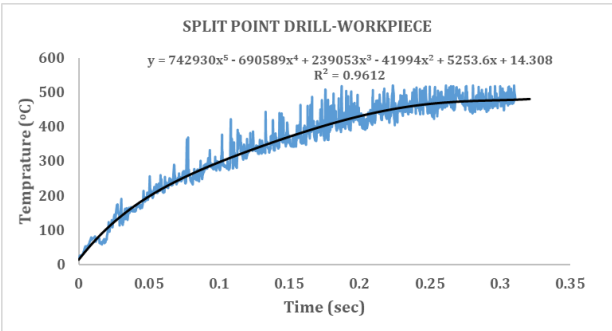

Fig. 9. Temperature generated on the workpiece during split point tip diving.

To begin with, it is obvious that both on the tool and the material processed the temperature is rising. This is because no coolant is used during drilling and due to large friction forces. Also, the minimum and maximum values for each component of the system are shown for a specific time step of the simulation. The spikes that exist in the plots are mainly caused from inaccuracies during the simulation, but they are of minor importance, and the temperature values are reliable, knowing the R^2 value. As seen for the tool, the temperature can reach approximately 140° C while on the workpiece it can get values about 500° C. This is presented on Fig. 10. Also, it can be seen that the improved rake geometry of the drill and the small chisel edge length gives the ability to cut material near the center of the drill.

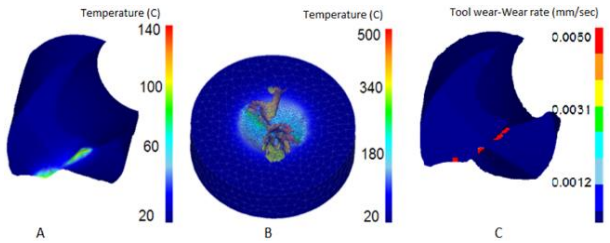

Fig. 10. Temperatures on the split point tip (A) and the workpiece (B) process and wear rate on the tool tip (C). In the workpiece the mesh with different size ratio is shown.

In Fig. 10 the wear rate of the drill is illustrated. If one thinks of the equation described on Usui's Wear model mentioned earlier, then it is clear that the causes of wear are the high temperatures generated, the high pressure needed for the operation to proceed and the sliding velocity.

The above results show that the drilling process has not reached a steady-state condition because the simulation regards mainly the centre of the tool.

4.2 Angled workpiece results

In this section, the whole tool tip geometry is simulated and evaluated.

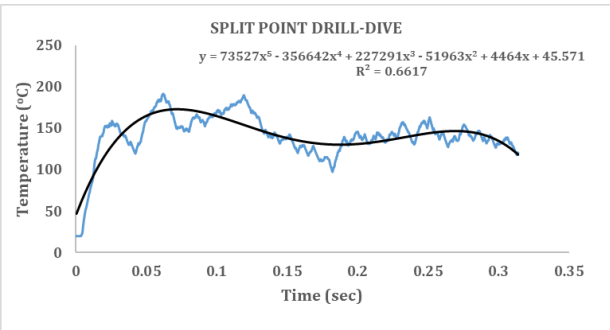

Fig. 11. Temperature generated on the split point drill tip during total cutting-edge length.

When the whole split point drill tip is subject to material cutting, the difference in temperatures is minor in comparison to the earlier type of simulation. Physically the contact area is larger, which leads to higher friction forces which as a result generate higher temperatures, but still close to the ones of the tip simulation. Namely, the temperature on the drill is close to 140° C and on the workpiece close to 500° C, which is seen on Fig. 11 and Fig. 12 respectively. Also, the chip shape generated is curly (Fig. 13), meaning that it breaks in small pieces and is removed easily from the drill's flutes.

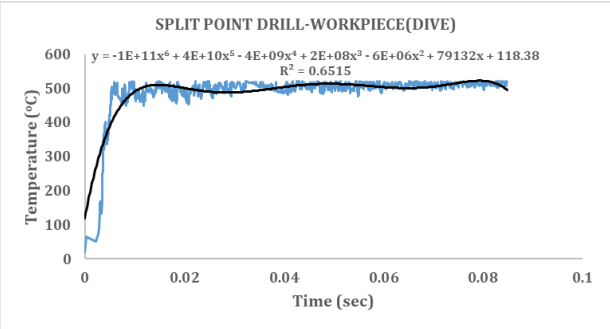

Fig. 12. Temperature generated on the workpiece during total cutting-edge length with the split point drill.

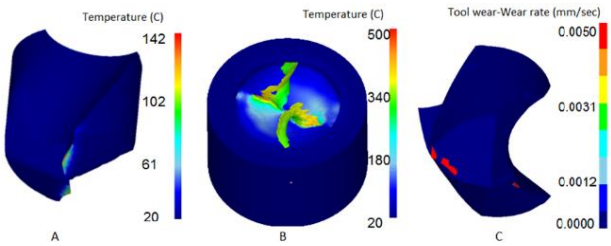

Fig. 13. Temperatures on the faces of the drill (A) and the workpiece surface (B) and wear rate on the tip of tool (C).

What is more interesting about the split point geometry is the fact that the temperature plots on both the tool and the workpiece tend to get a shallow slope. This means that the system starts to reach a steady state condition during machining. However, as there is no coolant during process except air, and knowing that the tool wear is gradually increasing, it is reasonable that always the temperature plots will show elevating temperatures. When the whole cutting edge of the drill is cutting material, the wear rate increases, and the areas that tend to be subject to higher friction and stresses, meaning the areas that will wear faster are the ones close to the drill's margins, as shown in Fig. 13.

Table 5: Cutting speeds and feeds for the new system.

Cutting conditions	Symbol	Values
Cutting speed (m/min)	Vc	90
Feed per revolution (mm/rev)	f_{rev}	0.25

In order to evaluate and estimate the above simulation findings, the second type of simulation is also examined regarding the thrust force that is required for the process of drilling. In addition to that, as a measure of comparison with the literature, the same model was also studied with the feeds and speeds shown below, in Table 5.

The results of the simulations models are shown below in Fig. 14. Bar 1 represents the simulation model with the feeds and speeds that are mentioned in Table 4, where the thrust force is close to 2950 N. Bar 2 shows the thrust that is required for the new model that is studied, where the cutting conditions are mentioned in Table 5. As indicated in the graph, the thrust that is required is increased a lot and is close to 3500 N. This is caused from the higher feed rate that is applied. Finally, bar 3 shows a simulation model that was studied in [12], where the cutting conditions that were used are the same with the ones mentioned in Table 5, the drill has similar characteristics (geometry and coating) with the current work and the workpiece is also H-13 steel. In this bar, the thrust is over 3600 N, and this is probably due to the fact that the tool is slightly larger in diameter (D=14 mm) in comparison to the current work, where the nominal diameter of the drill is D=10 mm. Nevertheless, it can be seen that there are no significant differences in the findings of the present work and the literature, which verifies the validity of the results presented earlier.

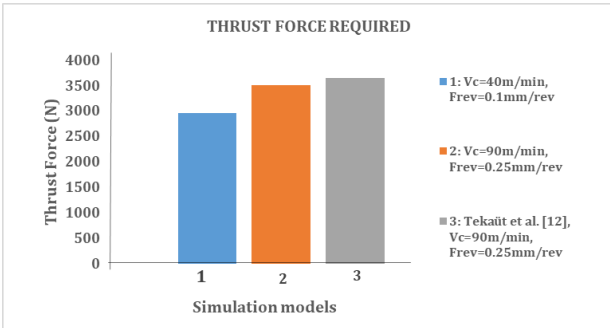

Fig. 14. Thrust force required for the 3 simulation models.

5. EXPERIMENT EVALUATION

In order to evaluate and ensure that the above simulations results were valid, an experiment was conducted in same cutting conditions such as those used is the software, in order to record the temperatures of the tools after the process.

A round bar of 120mm diameter and 55mm height H-13 was used as specimen. The surface where drilling was performed was grinded to provide the best available flatness, perpendicular to the drill. The drill used had the exact geometry with the one mentioned earlier

in order to have minimum deviations in the results. Also, the feeds and speeds were those mentioned in Table 4.

In addition, a thermal camera was used to record the temperatures after hole making. In order to ensure that the IR camera gives correct results, a calibration procedure according to the manufacturer recommendations was followed. At first, the camera's emissivity was set to 0.96. A test on boiling water was conducted for this purpose. Subsequently, a similar test was performed in measuring iced water. In both cases the camera gave correct temperatures, with an error of $\pm 3^{o}C$, which is within the manufacturer specs. The range of the camera is $-20^{o}C$ up to $400^{o}C$, and for the present experimental setup, the tool surface has 80% emissivity. In such type of machining process, a thermocouple would be physically impossible to be used, because drilling takes place in solid material, and there is no space for the thermocouple to be adhered properly on the tool cutting edges in order to yield adequate results.

In total 6 holes were made. Finally, the experiment was conducted on the machining shop facilities of University of Patras, with the use of a three axis CNC mill. The tool was tightened with use of a collet chuck, which provides minimum eccentricity during process, and sufficient rigidity. The part was also secured in appropriate way.

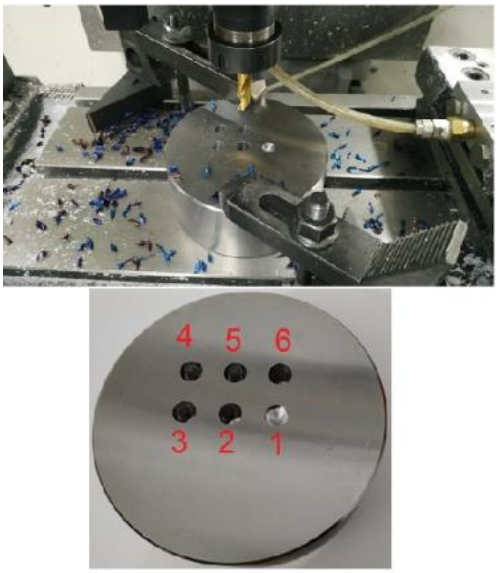

Fig. 15. Machine setup (up) and machined part (bottom).

In Fig. **15** the setup of the machine and the machined part are presented, with numbered holes. Each hole has a depth of $20mm$, except for the first one ($5mm$), which was used as a test for the setup of the machine and the tool. What is more, the holes were made with $20mm$ distance between them, in order to ensure that no material properties were changed due to high temperatures and material stresses.

When the drill starts to enter the workpiece, projection of the material takes place in the centre of the drill in the chisel edge area, generating high friction forces and temperatures. As the process continues, the rake faces of the drill dive in the workpiece, high shearing stresses and temperatures are presented, and the integrity of the material is changed. Chips of the workpiece are produced, leading to the creation of the hole. In the sequel, fragments of the chips are adhered on the tool, causing the creation of BUE. As the process continues, the newer formed chips are moving on the sliding region of the tool, which in other terms is the tool's rake faces and flutes. In this way the adhesive wear mechanism takes place. At this point, there is maximum interaction between the tool and the workpiece. On the margins of the drill, flaking is usual, as the edges of the cutting lips tend to be quite sharp. This means that along with the higher amount of material that needs to be removed during process, high stresses are presented on them. This leads to the flaking wear mechanism, where fragments of the margins are removed. The above are shown in the experiment observation (Fig. **17** and Fig. **18**), as well as in Fig. 10, Fig. 13, and Fig. **16**.

The results of the experiment showed good resemblance with the simulations. In Fig. **16**, the chips produced from the coated drill seem to be similar with the chips that are formed on the simulation of the tool. This is of prime concern, because small chips are easily disposed via the drills' flutes. In addition, the blueish colour of the chips shows that high thermal loads are also disposed via them, and not the material, which means that minimum stresses are shown on the machined part due to thermal loads, and minimum changes on its mechanical properties take place. However, here it is worth noticing that during machining, most of the shear stresses and friction generated are applied on the material that is removed, therefore it is reasonable for the chips to get elevated temperatures.

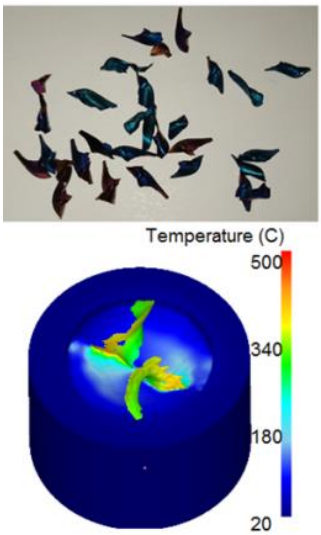

Fig. 16. Chip formation of the drill.

Concerning the temperatures, the drill yielded results closely correlated to the simulations. In Fig. **17**, the respective temperatures are illustrated. More specifically, the thermal camera used to record the temperature during machining showed the following results:

- 120° C on the third hole and
- 135° C on the fifth hole.

The temperatures calculated from the simulation models ranged approximately to 140° C. The differences on the model and the thermal camera were caused by the thermal camera's accuracy and calibration. Also, The temperature was measured 1.2sec after the experiment, which is the calculated time the machine needed for the tool to exit the workpiece.

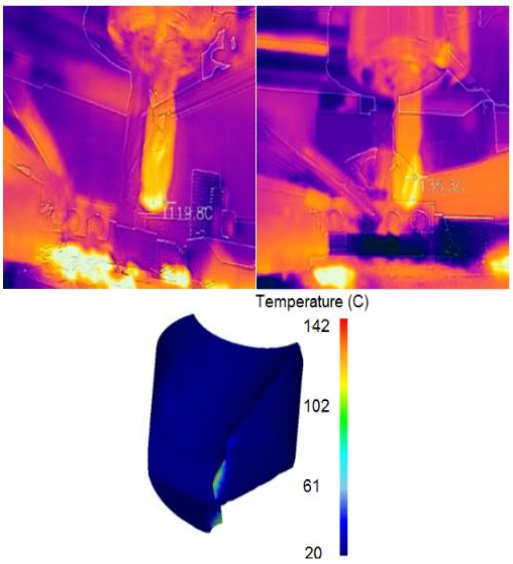

Fig. 17. Temperatures of the drill.

The data for the validation of the experiment can be compared to the experimental findings of [8]. Table 6 shows the temperatures obtained from the present model and experiment, as well as the temperatures measured in [8] for dry drilling in the same material with use of WC drills. It can be seen that the results obtained from the present models and experiment are in good agreement with the results of [8]. Higher deviation is found in the experimental temperatures recorded from the thermal camera, which are accepted due to the limitations mentioned earlier.

Table 6: Temperatures of drilling processes.

Drilling process	Temperatures (^{o}C)
Experiment	120-135
Model	~140
Brandao et.al [8]	~142

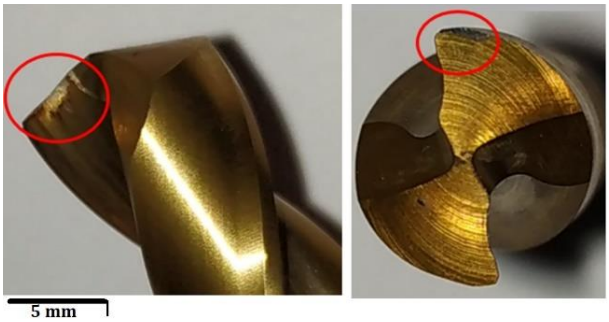

Fig. 18. Rake face (left) and margin wear (right) on the tool.

Finally, the wear of the drill can be physically evaluated. In Fig. **18** it is shown that the drill's rake faces start to wear out, meaning that the coating starts to fade. Similar results were shown in the simulation models (Fig. 10 and Fig. 13). This type of wear is shown on both cutting faces of the drill due to its symmetry. It is mainly caused from adhesion of the material processed on the rake faces, which forms BUE and when it is removed it also detaches part of the coating with it. Also, in the same figure, a fragment of the drill's margin is missing, and this is caused by flaking as it was revealed earlier. In addition, the chisel edge and flank faces show minimum wear. In the Introduction, the reviewed literature showed that drills tend to wear relatively easily towards the periphery of their cutting edges where the rake angles are more 'aggressive', while chisel edge resists more. Apart from that, the literature suggests that the flank faces were also prone to wear, either from adhesion or

other types, but the results of this study cannot confirm this phenomenon due to the high clearance angles of the drill, and the fact that the tool was not used for prolonged periods of time.

Overall, the above experiment and simulation findings are attested with a comparison with the literature, knowing that the rake faces of the coated drill are grinded in such way to keep their high positive value even close to the center of the drill (chisel edge).

5.1 Chip microstructural analysis

The microstructural analysis of the produced chips verifies the adhesive wear mechanism during the process of drilling.

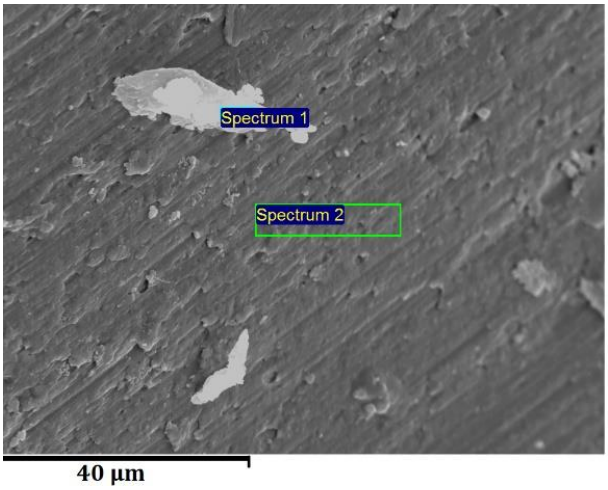

Fig. 19. Scanning electron microscope (SEM) view of produced chip.

In the above illustration (Fig. 19), the surface of produced chip is shown. It regards the tool-chip interface, where sliding of the chip takes place. In this region of the tool, rake face wear is presented. Spectrum 1 and Spectrum 2 chemical elements are shown in Fig. 20 and Fig. 21 respectively. In both figures, a high value of Au is presented. This is caused from the fact that the chips were gold plated for better operation of the microscope. In Spectrum 1 there are signs of Ti, which indicates that fragments of the tool's coating exist on the produced chip. As mentioned earlier, this is called adhesion, and is a wear mechanism that is applied on the current work. On the other hand, in Spectrum 2 the main chemical elements of Orvar are present.

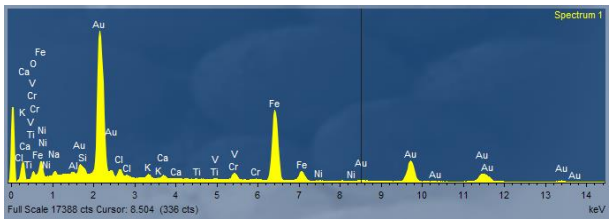

Fig. 20. SEM mapping (Spectrum 1).

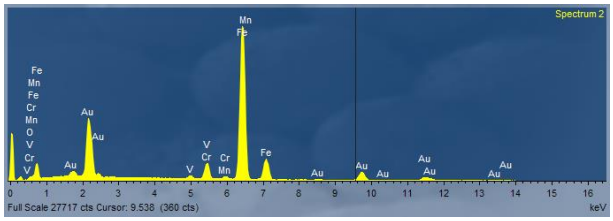

Fig. 21. SEM mapping (Spectrum 2).

In Fig. 22 the 'inside' surface of the chips is presented. Unlike Fig. 19, it is evident that no sliding takes place, and the surface of the chip seems to be fibrous.

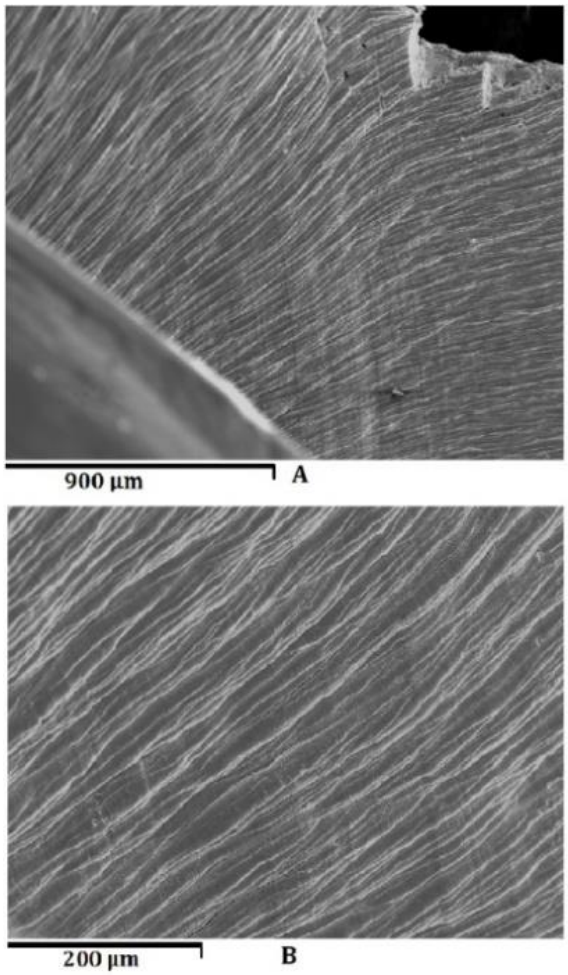

Fig. 22. SEM images of the colored zone close to the sharp end of the drill after 6 holes and cutting speed, Vc =40 m/min.

It is typical for the chips to form fibrous, or in other words a 'wiring' shape. The material tends to be aligned towards the direction the cutting forces are applied. In this way shearing takes place, and severe plastic deformation occurs.

6. CONCLUSION

In this paper, a numerical and experimental procedure was presented. The finite element method was used in order to simulate the cutting forces, as well as the temperatures and the wear rate that occur in drilling processes. An Orvar piece and a TiN coated drill was used to simulate the process. An experiment was performed, regarding temperature measurements and SEM microscopy for the drill's coating characterization.

The maximum wear rate for the drill on both simulation setups was around $0.005\,\mathrm{mm/sec}$. This value was obtained for maximum tool temperature, which was predicted close to $140^{o}\,\mathrm{C}$. The main wear mechanisms are adhesion and abrasion, while the high thermal loads are applied in both the tool and the workpiece. The shallow temperature slope shows a tendency to reach a thermal steady state condition as drilling proceeds. Due to the relatively low wear rate and low temperatures, the coated drills for the dry drilling of tough alloys such us H-13, is a very effective option. Finally, it can be concluded that the implemented approach provides an efficient method for other dry drilling processes to increase their performance and reduce the possible production defects.

The elasticity of the drill and the temperature measurements directly, close to drill tip are two of the limitations of the proposed methodology. In conclusion, the use of the nanostructure materials as coatings and the investigations of the chemical properties of the materials during drilling such as the oxidation and the effects of lubrication/cooling in elevated temperatures could be topics on which future research can be focused.

Acknowledgement

The authors wish to acknowledge all the support provided from the Machine Design Laboratory of Department of Mechanical Engineering and Aeronautics, machine shop and Laboratory of Electron Microscopy and Microanalysis of University of Patras. In addition, the authors would like to express their gratitude to Aikaterini Govatsi, Maria S. Panagopoulou for their valuable contribution and support throughout this study and to Zikos Metallurgy S.A. for the provision of all of the needed experimental materials.

REFERENCES

[1] H.K. Tönshoff, W. Spintig, W. König A. Neises, *Machining of Holes Developments in Drilling Technology*, CIRP Annals, vol. 43, iss. 2, pp 551–561, 1994, doi: 10.1016/S0007-8506(07)60501-0

[2] E.O. Ezugwu, C.J. Lai, *Failure modes and wear mechanisms of M35 high-speed steel drills when machining inconel 901*, Journal of Materials Processing Technology, vol. 49, iss. 3–4, pp 295-312, 1995, doi: 10.1016/0924-0136(94)01352-2

[3] Y. C Chen, Y.S. Liao, *Study on wear mechanisms in drilling of Inconel 718 superalloy*, Journal of Materials Processing Technology 140, vol. 140, iss. 1–3, pp 269-273, 2003, doi: 10.1016/S0924-0136(03)00792-1

[4] F. Jafarian, H. Samarikhalaj, *Experimental Investigation and Optimizing Geometrical Characteristics and Surface Quality in Drilling of AISI H13 Steel*, Journal of Applied and Computational Mechanics, vol. 6, iss. 2, pp 332-343, 2020, doi: 10.22055/JACM.2019.29070.1552

[5] J. Ganesh, P. Renukadevi, P. Vijayakumar , *Experimental optimization of drilling process parameters on die steel (H13) using carbide coated drill by Taguchi design method*, International Journal of Mechanical Engineering and Technology, vol. 8, iss. 3, pp 159–167.

[6] I. Tekaüt, H. Demir,U. Şeker, *The relationship of cutting force with hole quality in drilling process of AISI H13 steel*, MATEC Web of Conferences, vol. 129, article 01042, 2017, doi: 10.1051/matecconf/201712901042

[7] I. Tekaüt, H. Demir. *The effects of cutting tool coating and machining parameters in drilling of steel AISI H13 and AISI D2*, Journal of the Faculty of Engineering and Architecture of Gazi University, vol. 30 iss.2, pp. 289-296, 2015.

[8] L.C. Brandao, R.T. Coelho, C.H. Lauro, *Contribution to dynamic characteristics of the cutting temperature in the drilling process considering one dimension heat flow*, Applied Thermal Engineering, vol. 31, iss. 17–18, pp 3806-3813, 2011, doi: 10.1016/j.applthermaleng.2011.07.024

[9] L.C. Brandão, F. Neves, G. Orio, C. Nocelli,

Evaluation of Hole Quality in Hardened Steel with High-Speed Drilling Using Different Cooling Systems, Advances in Mechanical Engineering, vol. 3, pp. 1–7, 2011, doi: doi.org/10.1155/2011/746535

[10] C.H. Lauro, L.C. Brandao, T.J.S. Vale, A.L Christoforo, *An approach to define the heat flow in drilling with different cooling systems using finite element analysis,* Advances in Mechanical Engineering, vol. 5, pp. 1–9, 2013, doi: 10.1155/2013/612747

[11] H. Coldwell, R. Woods, M. Paul, P. Koshy, R. Dewes, D. Aspinwall, *Rapid machining of hardened AISI H13 and D2 moulds, dies and press tools*, Journal of Materials Processing Technology, vol. 135, iss. 2–3, pp 301-311, 2003, doi: 10.1016/S0924-0136(02)00861-0

[12] I. Tekaüt, H, Demir, U. Şeker, Experimental *Analysis and Theoretical Modelling of Cutting Parameters in the Drilling of AISI H13 Steel with Coated and Uncoated Drills*, Transactions of FAMENA, vol. 42, no. 2, pp 83–96, 2018, doi: 10.21278/TOF.42207

[13] J. Wu, R.D. Han, *A new approach to predicting the maximum temperature in dry drilling based on a finite element model*, Journal of Manufacturing Processes, vol. 11, iss. 1, pp. 19–30 , 2009, doi: 10.1016/j.jmapro.2009.07.001

[14] M. Bono, J. Ni, *The location of the maximum temperature on the cutting edges of a drill*, International Journal of Machine Tools and Manufacture, vol. 46, iss. 7–8, pp. 901-907, 2006, doi: 10.1016/j.ijmachtools.2005.04.020

[15] J. Lorentzon, N. Järvstråt, *Modelling tool wear in cemented-carbide machining alloy 718*, International Journal of Machine Tools and Manufacture, vol. 48, iss. 10, pp. 1072-1080, 2008, doi: 10.1016/j.ijmachtools.2008.03.001

[16] Q . Zhang, *A Study of High Performance Twist Drill Design and the Associated Predictive Force Models,* PhD thesis, School of Mechanical & Manufacturing Engineering, University of New South Wales, 2007.

[17] S. Zhang, W. Zhu, *TiN coating of tool steels: a review*, Journal of Materials Processing Technology, vol. 39, iss. 1–2, pp 165-177, ISSN 0924-0136, 1993 doi: 10.1016/0924-0136(93)90016-Y

[18] E. Armarego, *The unified-generalised mechanics of cutting approach - A step towards a house of predictive performance models for machining operations*, Machining science and technology, vol. 4, iss. 3, pp. 319–362, 2000, doi: 10.1080/10940340008945715

[19] W.J. Endres, R.E. DeVor, S.G. Kapoor, *A Dual-Mechanism Approach to the Prediction of Machining Forces, Part 2: Calibration and Validation*, Journal of Manufacturing Science and Engineering, vol. 117, iss. 4, pp. 534–541, 1995, doi: 10.1115/1.2803531

[20] J.F. Archard, *Contact and Rubbing of Flat Surfaces*, Journal of Applied Physics, vol. 24, iss. 8, pp. 981-988,1953, doi: 10.1063/1.1721448

[21] K. Kato, K. Adachi, *Wear mechanisms*, in Modern Tribology Handbook, vol. 1, CRC Press, pp. 273–300, 2001.

[22] E. Usui, T. Shirakashi, T. Kitagawa, *Analytical prediction of cutting tool wear*, Wear, vol. 100, iss. 1–3, pp. 129-151, ISSN 0043-1648, 1984, doi: 10.1016/0043-1648(84)90010-3

[23] A. Dahlström, *Wear Mechanisms in Austenitic Stainless Steel Drilling : A Comprehensive Wear Study*, Master thesis, School of Industrial Enginnering and Management, Royal Institute of Technology, Stockholm, 2015.

[24] V.P. Astakhov, *Tribology of Metal Cutting*, Elsevier Science, 2006

[25] Orvar steel properties available at http://www.uddeholm.com/, accesed 5.12.2020.

[26] U.C. Berkeley, D. Joel, J. Gardner, D. Dornfeld, *Finite Element Modeling of Drilling Using DEFORM*, Consortium on Deburring and Edge Finishing Publication, Laboratory for Manufacturing and Sustainability, 2006.

NOMENCLATURE

D Nominal diameter (mm)

$2p$ Point angle (deg)

ψ Chisel edge angle (deg)

$2W$ Web thickness (mm)

$2W/D$ Web thickness ratio

δ_0 Helix angle (deg)

α_0 Lip clearance angle (deg)

Vc Cutting speed (m/ min)

f Feed rate (mm/ min)

f_{rev} Feed rate (mm/ rev)

H_c Hardness of coating (kg/ mm^2)

H_f Hardness of film (kg/ mm^2)

H_s Hardness of substrate (kg/ mm^2)

V_f Deformation volume of film (mm^3)

V_s Deformation volume of substrate (mm^3)

V_t Total volume (mm^3)

c Interface parameter

F_p , F_q , F_r Force components (N)

b Width of cut (mm)

t Cut thickness (mm)

C_{ep} , C_{eq} Edge force coefficients

r_i Chip length ratio

β Friction angle (deg)

γ_n Normal rake angle (deg)

λ_s Inclination angle (deg)

τ Shear stress in shear zone (Mpa)

μ Friction coefficient

F_a Normal force (N)

F_N Friction force due to F_a (N)

τ_i Shear stress on the contact surface (Mpa)

σ_N Normal contact pressure (Mpa)

V Worn volume (mm^3)

W_1 Normal load (N)

L Sliding distance (m)

H Hardness Brinell (kg/mm^2)

W Wear (mm/sec)

σ_t Normal stress (Mpa)

C_x Experimentally calibrated constants

θ Temperature ($^\circ C$)

VB Wear Volume (mm)

R_p Yield strength (Mpa)

R_m Tensile strength (Mpa)

N Revolutions per minute (rpm)

σ Flow stress (Mpa)

A Yield stress (Mpa)

B Strain hardening factor

n Strain hardening index

C Strain rate sensitivity parameter

T Homologous temperature ($^\circ C$)

m Thermal softening coefficient

T_r Ambient temperature (^oC)

T_m Melting temperature of material (^oC)